J Intell Robot Syst (2015) 78:577–591
DOI 10.1007/s10846-014-0087-9

A Kalman-filtering-based Approach for Improving Terrain Mapping in off-road Autonomous Vehicles

Isao Parra-Tsunekawa · Javier Ruiz-del-Solar · Paul Vallejos

Received: 4 February 2014 / Accepted: 15 July 2014 / Published online: 1 August 2014
© Springer Science+Business Media Dordrecht 2014

Abstract The generation of accurate terrain maps while navigating over off-road, irregular terrains is a complex challenge, due to the difficulties in the estimation of the pose of the laser rangefinders, which is required for the proper registration of the range measurements. This paper addresses this problem. The proposed methodology uses an Extended Kalman filter to estimate in real-time the instantaneous pose of the vehicle and the laser rangefinders by considering measurements acquired from an inertial measurement unit, internal sensorial data of the vehicle and the estimated heights of the four wheels, which are obtained from the terrain map and allow determination of the vehicle's inclination. The estimated 6D pose of the laser rangefinders is used to correctly project the laser measurements onto the terrain map. The terrain map is a 2.5D map that stores in each cell the mean value and variance of the terrain height. In each map's cell position, new laser observations are fused with existing height estimations using a Kalman filter. The proposed methodology is validated in the real world using an autonomous vehicle. Field trials show that the use of the proposed state estimation methodology produces maps with much higher accuracy than the standard approaches.

Keywords Terrain mapping · Off-road autonomous vehicles · Kalman Filter · Information fusion · Laser rangefinder pose estimation

I. Parra-Tsunekawa · J. Ruiz-del-Solar (✉)
Department of Electrical Engineering,
Universidad de Chile, Santiago, Chile
e-mail: jruizd@cec.uchile.cl

I. Parra-Tsunekawa
e-mail: sparra@ing.uchile.cl

I. Parra-Tsunekawa · J. Ruiz-del-Solar · P. Vallejos
Advanced Mining Technology Center,
Universidad de Chile, Santiago, Chile
e-mail: pavallej@ing.uchile.cl

1 Introduction

Terrain mapping is a relevant problem in autonomous robot navigation; the accurate modeling of the terrain is required for the robot in order to decide a safe path to follow. In off-road applications, the generation of accurate terrain maps while navigating is a difficult challenge due to the difficulties in estimating the pose of the laser rangefinders, which is required for the proper registration of the range measurements. Even small pose errors could be magnified onto large errors in the projected positions of laser points, because the laser rangefinders are aimed at the road up to several meters in front of the vehicle [13].

We address the problem of real-time terrain mapping for autonomous vehicles such as cars and trucks that move at low (<10[m/s]) and medium speeds (<20[m/s]) for off-road terrain applications, as in the case of the autonomous truck operation in open pit

mines, where typical speeds are in the range of 5-14 [m/s]. We address the specific problem of building coherent semi-local terrain maps with laser range finders whose 6D pose changes due to the irregular surface that the vehicle is traversing and the non-rigid characteristics of the vehicle (vehicle suspension system). We use the term semi-local map to denote a map that: (1) is built without using GPS information, (2) uses a global reference system that is defined at the beginning of the map estimation, (3) has an extension of several hundred meters, and (4) can be integrated onto the global map using the GPS and inertial data. We use semi-local maps because we are interested in achieving a very accurate 6D pose estimation of the laser range finders; the use of standard GPS (no differential) in this estimation process would produce inaccuracies that would be reflected in the generated map. The semi-local map can be used for taking local decision (obstacle avoidance, decision about which path to follow) and/or for building the global map.

The proposed methodology uses an Extended Kalman filter for estimating in real-time the instantaneous pose of the vehicle and the laser rangefinders by considering measurements (observations in the Kalman filtering terminology) acquired from an inertial measurement unit (3D angular pose and speed, and 3D linear acceleration), internal sensorial data of the vehicle (vehicle speed and angle of the steering wheel) and the estimated heights of each wheel, which are obtained from the terrain map and allow determining the vehicle's inclination. The estimated 6D pose of the laser rangefinders is used to correctly project the laser measurements onto the terrain map. The terrain map is a 2.5D map that stores the mean value and variance of the terrain height. In each map's cell position, new laser observations are fused with existing height estimations using a Kalman filter.

The main contribution of this work is the proposal of an integrated sensor-map estimation methodology in which: (i) Kalman filters estimate the laser range finder 6D pose and fuse past and new observations in each cell of the terrain map and (ii) the estimated terrain map is fed back and used for improving the 6D pose estimation of the laser range finders (past estimations of the terrain heights are used for determining the current heights of the wheels and therefore the inclination of the vehicle).

The methodology is validated in the real world (O'Higgins Public Park, located near downtown area in Santiago de Chile, Chile), using the AMTC's autonomous vehicle. Field trials show that the use of the proposed state estimation methodology produces maps with higher accuracy than approaches that use the inertial data directly (without any state estimator) for correcting the pose of the laser range finders.

The paper is organized as follows: Related work is described in Section 2; The proposed Kalman-filtering based methodology for terrain mapping is explained in Section 3; Descriptions of experiments and results are presented in Section 4 and Conclusions of this work are given in Section 5.

2 Related Work

Terrain map estimation is an important component in outdoor mobile robot navigation, and several authors have addressed it ([2–13]). Some of them have concentrated their effort on the fusion problem [12] while others have addressed the representation of the terrain data within the map [5] or the use of elevation functions over a 2D domain to represent the map [3]. Other authors have tackled the filtering of the laser range finder data to improve map quality [8], the assessment of the traversability of the terrain [9], the accurate registration of the laser range finder data [10–13] or the loop-closing problem when building a global map [5]. Some of these works use small rovers in the experiments or cars moving at low speeds (<10 [m/s]) while in some cases the map is built offline [5].

Different types of representations have been used to map terrains (e.g., 2D occupancy grid, 3D occupancy voxel), being the elevation or 2.5D height map one of the preferred options in ground robot mapping applications (for example [10–12]) due to their compactness, lower computation and insensitivity to height discretization errors [12]. Elevation maps "store in each cell of a discrete grid the height of the surface at the corresponding place in the environment" [5]. In some mapping systems the height's variance is also stored in each cell [10, 11].

The estimation of the terrain height in each cell in a 2.5D map requires the correct fusion of measurements obtained at multiple times while moving. The uncertainty of the measurements and the uncertainty of the sensor pose must be considered during the fusion process. This is addressed in [10] by proposing a mixture-model terrain estimation framework

that incorporates both uncertainties, together with the measurement-map association and the in-cell measurement fusion into the map. The terrain mapping and estimation algorithm uses a probabilistic analysis of the errors, assuming their Gaussian distribution. The system projects the sensors's detections onto the global coordinate frame using a tightly coupled model of the sensors position, making the respective formal error propagation. The vehicle localization is obtained from a GPS, without the use of any state estimation algorithm

In [11], three enhancements were proposed for improving the real-time performance of the system proposed in [10]: a selection window was used to limit the probability distribution area of each measurement, a clustering algorithm was used to simplify the object detection tasks and a virtual point vector was introduced to reduce the computational cost of the algorithm. Despite these enhancements, no fundamental changes were made to the terrain estimation framework proposed in [10].

In [12], a Markov Random Field (MRF) representation of a sensor and terrain fusion model was proposed. The MRF represents the model of 2.5D map sensor uncertainties, enabling a probabilistic fusion between the sensor and terrain information. This approach is also based on [10], but it does not make the assumption of independency among cells in the map.

In Thrun [13], a first-order Markov model is proposed for modeling the drift of the pose estimation error over time. The heights of the map points are assumed Gaussian with a variance that scales linearly with the time difference of the points. Then, a probabilistic test is used to detect the presence of an obstacle. Thus, that work focuses on the detection of obstacles rather than on providing an accurate map. The methodology proposed in this publication addresses both problems; it is able to compute an accurate semi-local map in real-time, which can be then used for obstacle avoidance.

The main difference of the current methodology compared with [10–13] is that in the methodology proposed in this paper, a non-rigid sensor location and vehicle suspension is assumed. Therefore, the noise in the sensor pose associated with the sensor and vehicle vibration is explicitly considered. This vibration is estimated in real-time using the Inertial Measurement Unit (IMU) measurements. Furthermore, the vehicle pose is estimated using an Extended Kalman filter, avoiding the extreme dependency upon the GPS that most terrain map estimation systems have.

In [5], an approach that allows a mobile robot to deal with vertical and overhanging objects in elevation maps is presented. The approach uses four classes (traversable cells, vertical gaps, vertical structures and locations sensed from above) for classifying locations in the environment and dealing with overhanging structures. The map of elevations is updated using a Kalman filtering fusion approach (in each cell new data is fused with existing estimations by considering their variances). In that work the loop closing in the map is solved offline and the vehicle moves on paved roads at low speeds.

In [6], a near real-time ground segmentation system based on Gaussian Process for autonomous land vehicle is proposed. Terrain is segmented into ground and non-ground, and the average processing time is 74.93 [ms], being near real-time. Terrain mapping systems built using the methodology proposed in this paper are able to process the data in real-time, having a processing time of $\sim$3 [ms] (see Section 4.3).

In summary, one of the main contributions of this work is the proposal of a real-time terrain map estimation system enhanced by the estimation of the noise produced by the sensors and vehicle vibration, its use in the measurement fusion process, and the estimation of the vehicle and sensors pose without the GPS dependency.

3 A Kalman-Filtering Based Methodology for Terrain Mapping

3.1 System Overview

The proposed methodology for terrain mapping has three main stages: *Vehicle State Estimation*, *Laser Projection* and *Terrain Map Update* (see block diagram in Fig. 1). The first stage estimates the full 6D pose of the vehicle using an Extended Kalman filter. For correcting the predicted pose, it uses: (i) observations acquired from the IMU, (ii) vehicle internal sensors whose measurements are available in the CAN bus (Controller Area Network), and (iii) virtual observations obtained from the terrain map. The second stage generates a projection of the laser rangefinders measurements onto a global reference system using the 6D pose of the laser rangefinders, which is

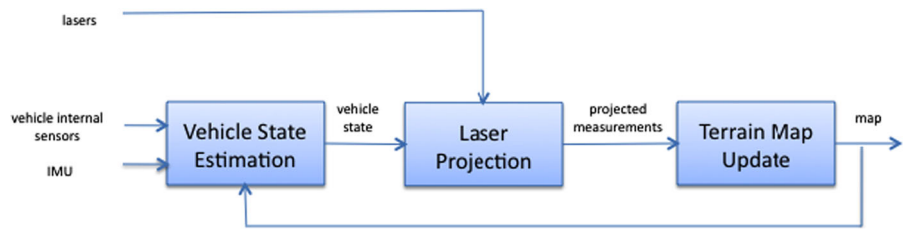

Fig. 1 Block diagram of the proposed estimation system

computed from the vehicle's pose. Finally, the *Terrain Map Update* stage accumulates the laser observations in the terrain map. The terrain map stores, in each cell, the mean value and variance of the terrain height. A Kalman filter is used in each cell for fusing new laser observations with existing height estimations.

3.2 Vehicle Model

A simplified diagram of the vehicle model is shown in Fig. 2. The vehicle model corresponds to a standard four-wheel front-steering vehicle with laser rangefinders and an IMU mounted on a roof rack. The distance between the front and rear axes is called the *wheelbase*, while the distance between the steerable wheels is known as the *track*. The vehicle kinematics is given by the following variables (see reference systems in Fig. 2): global position $\vec{p}_t$, 3D angular pose $\vec{q}_t$, speed v_t, instantaneous rotation radius r_t, angular speed ω_t, and steer angle α_t. The angle α_t is defined as the equivalent steer angle of a bicycle with both the same *wheelbase* and r_t as the actual vehicle. This angle is related to the steer angles of the inner and outer wheels, α_t^i and α_t^o respectively, as shown in Eq. (1) [1],

$$\cot \alpha_t = \frac{\cot \alpha_t^o + \cot \alpha_t^i}{2} \tag{1}$$

The variables $\vec{p}_t$ and $\vec{q}_t$ are measured in the global reference system S_G, with the x axis pointing towards the east, the y axis point towards the north and the z axis pointing upwards. θ, ϕ, and ψ denote rotation angles around the x, y and z axes, respectively.

3.3 Sensor Models and Variables

The following information sources are used in the vehicle: an IMU, laser rangefinders and internal sensors data (e.g., speed) that is measured by the vehicle itself and that is available in the CAN bus.

The IMU provides the following data: angular pose $\vec{\vartheta}_t^{\,imu} \in \mathbb{R}^3$, angular speed $\vec{\omega}_t^{\,imu} \in \mathbb{R}^3$ and linear acceleration $\vec{a}_t^{\,imu} \in \mathbb{R}^3$

By considering a laser reference system S_{laser} (see Fig. 2b), a laser rangefinder provides a sequence of measurements in polar coordinates $\vec{\rho}_{t,i}^{\,laser} = \left[\, d_{t,i} \;\; \theta_{t,i} \,\right]^T ; i \in \left\{1, ..., N_{samples}\right\}$, where: $d_{t,i}$ is the measured distance, $\theta_{t,i}$ the measured angle and $N_{samples}$ the number of samples at time step t. In case that more than one laser rangefinder is used, the index j will be used to identify laser rangefinder number j, as in $d_{t,i}^j$

The data provided by the internal sensors of the vehicle through the CAN bus interface are the angle of the steering wheel $\alpha_t^{vehicle}$ and the linear speed of the wheels $\vec{v}_t^{\,vehicle} \in \mathbb{R}^4$. This vector contains the speed of the front-left, front-right, rear-left and rear-right wheels.

3.4 Vehicle State Estimation

The state vector $\vec{x}_t$ includes all relevant variables that define the state of the vehicle:

$$\vec{x}_t = \left[\, \vec{p}_t \;\; \vec{q}_t \;\; v_t \;\; \alpha_t^{wheel} \;\; \eta_t \,\right]^T \tag{2}$$

with $\vec{p}_t$ a 3D-vector representing the position of S_L relative to S_G, $\vec{q}_t$ a quaternion representing the orientation of S_L relative to S_G, v_t a scalar representing the speed, α_t^{wheel} a scalar representing the angle of the steering wheel, and η_t the variance of the vehicle's vibration in the z axis. The problem of state estimation is solved in this case through the implementation of a Kalman filter.

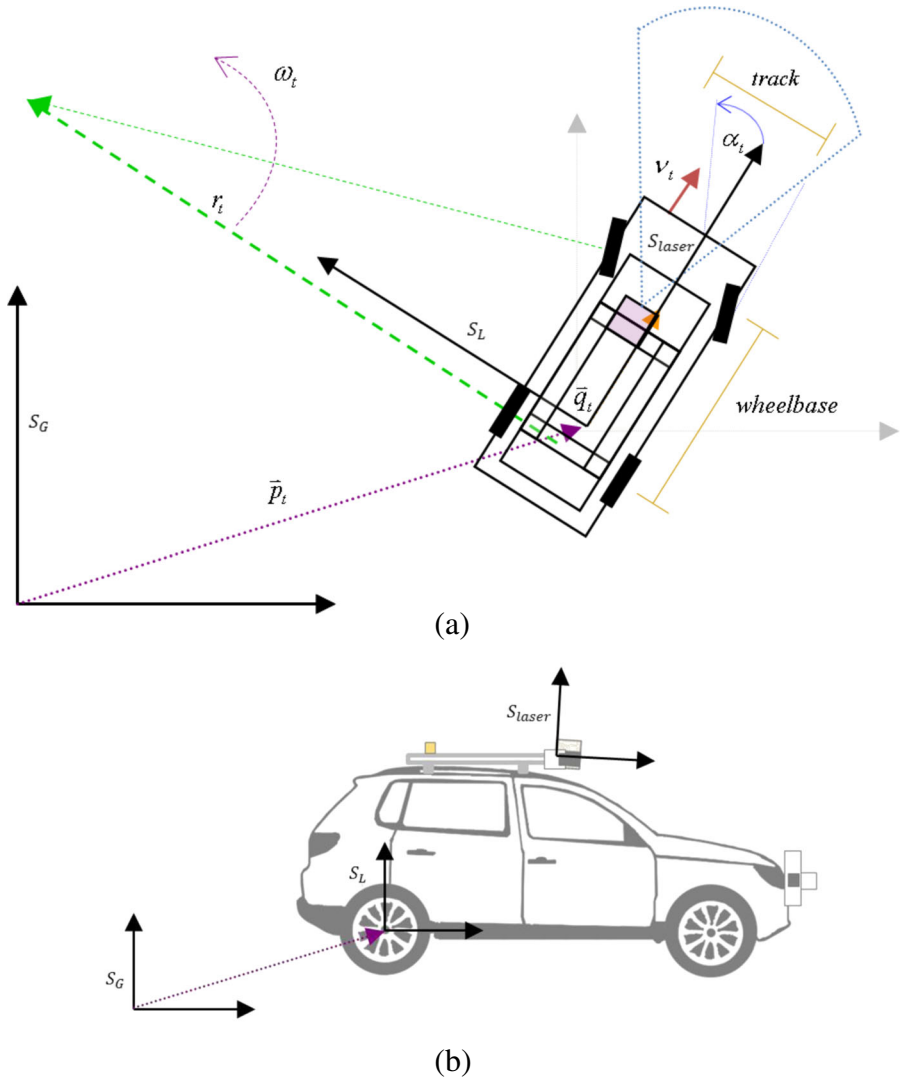

Fig. 2 Geometry, reference systems, and relevant variables (see main text for details): **a** Top and **b** lateral views

3.4.1 Extended Kalman Filter: Prediction Step

For the prediction step of the Extended Kalman filter, the following standard equations are used:

$$\begin{aligned} \vec{x}_t^- &= f\left(\vec{x}_{t-1}, \vec{u}_t, 0\right) \\ P_t^- &= A_t \cdot P_{t-1} \cdot A_t^T + Q \end{aligned} \tag{3}$$

with A_t the Jacobian matrix of partial derivatives of f with respect to $\vec{x}_t$, Q the process noise covariance and $\vec{u}_t$ the actuation order. The process noise is characterized and Q is estimated by means of field trial experiments.

In our model $\vec{u}_t$ is supposed unknown[1] and f is given by:

$$\begin{aligned} \vec{p}_t^- &= \vec{p}_{t-1} + \vec{q}_{t-1} \cdot \Delta\vec{p}_t \cdot \vec{q}_{t-1}^* \\ \vec{q}_t^- &= \vec{q}_{t-1} \circ \Delta\vec{q}_t \\ v_t^- &= v_{t-1} \\ \alpha_t^{wheel\,-} &= \alpha_{t-1}^{wheel} \\ \eta_t^- &= \eta_{t-1} \end{aligned} \tag{4}$$

[1]Even though, $\vec{u}_t$ is known when the vehicle operates autonomously, we decided to estimate the pose change in order to have a more general model and a more robust system; in many situations, such as, vehicle slippage, there is a significant difference between the given and executed orders.

with $\Delta\vec{p}_t$ and $\Delta\vec{q}_t$ the 3D position and orientation change, respectively; $\Delta\vec{q}_t$ is a quaternion.

The change of the vehicle's position, in the local/vehicle reference system S_L, is computed as:

$$\Delta\vec{p}_t = \begin{cases} \begin{pmatrix} r_t \sin(\omega_t \cdot \Delta t) \\ r_t(1-\cos(\omega_t \cdot \Delta t)) \\ 0 \end{pmatrix} & if\, \alpha_t^{wheel} \neq 0 \\ \begin{pmatrix} v_t \cdot \Delta t \\ 0 \\ 0 \end{pmatrix} & if\, \alpha_t^{wheel} = 0 \end{cases} \tag{5}$$

with r_t and ω_t the estimated rotation radius and speed and Δt the time interval.

The trajectory of the vehicle in Δt is approximated as circular, and ω_t and r_t are approximated using the estimated steering wheel angle and linear speed (see derivation in Appendix 1) as:

$$\begin{aligned} \omega_t &\simeq v_t \cdot \alpha_t^{wheel} \cdot \gamma \\ r_t &= \tfrac{v_t}{\omega_t} \simeq \tfrac{1}{\alpha_t^{wheel} \cdot \gamma} \end{aligned} \tag{6}$$

with γ an adjusting factor that depends of the vehicle. As mentioned, in case when $\alpha_t^{wheel} = 0, \omega_t = 0$ and $r_t = \infty$, and the trajectory is approximated as a straight line.

The angular pose difference is computed as:

$$\Delta\vec{q}_t = q_{YPR}(\omega_t \cdot \Delta t, 0, 0) \tag{7}$$

with q_{YPR} given by:

$$q_{YPR}(\psi, \varphi, \theta) = \begin{bmatrix} \cos\left(\frac{\theta}{2}\right)\cdot\cos\left(\frac{\varphi}{2}\right)\cdot\cos\left(\frac{\psi}{2}\right) + \sin\left(\frac{\theta}{2}\right)\cdot\sin\left(\frac{\varphi}{2}\right)\cdot\sin\left(\frac{\psi}{2}\right) \\ \sin\left(\frac{\theta}{2}\right)\cdot\cos\left(\frac{\varphi}{2}\right)\cdot\cos\left(\frac{\psi}{2}\right) - \cos\left(\frac{\theta}{2}\right)\cdot\sin\left(\frac{\varphi}{2}\right)\cdot\sin\left(\frac{\psi}{2}\right) \\ \cos\left(\frac{\theta}{2}\right)\cdot\sin\left(\frac{\varphi}{2}\right)\cdot\cos\left(\frac{\psi}{2}\right) + \sin\left(\frac{\theta}{2}\right)\cdot\cos\left(\frac{\varphi}{2}\right)\cdot\sin\left(\frac{\psi}{2}\right) \\ \cos\left(\frac{\theta}{2}\right)\cdot\cos\left(\frac{\varphi}{2}\right)\cdot\sin\left(\frac{\psi}{2}\right) - \sin\left(\frac{\theta}{2}\right)\cdot\sin\left(\frac{\varphi}{2}\right)\cdot\cos\left(\frac{\psi}{2}\right) \end{bmatrix} \tag{8}$$

The estimation of the noise covariance matrix Q considers the following elements: (i) it is assumed that the noise components are not correlated and therefore that Q is diagonal, (ii) the variance of the different components is estimated using the technical specifications of the sensors (IMU's accelerometers and gyroscopes, internal sensors of the vehicle) and the vehicle's speed range given by the application, and (iii) a proper error projection of the angular errors to the quaternion space.

3.4.2 Extended Kalman Filter: Correction Step

For the correction step of the Extended Kalman filter, the following standard equations are used:

$$\begin{aligned} K_t &= P_t^- H_t^T \left(H_t P_t^- H_t^T + R_t\right)^{-1} \\ \vec{x}_t &= \vec{x}_t^- + K_t\left(z_t - h(\vec{x}_t^-)\right) \\ P_t &= (I - K_t H_t) P_t^- \end{aligned} \tag{9}$$

with H_t the Jacobian matrix of partial derivatives of h with respect to $\vec{x}_t^-$, R_t the measurement noise covariance matrix and K_t the Kalman gain.

The corrections are done sequentially using the perceptual data obtained from the IMU and the vehicle internal sensors as well as using virtual observations obtained from the map of elevations, which is considered as a soft sensor.

In our modeling, we choose to transform the different measured variables (e.g., angular speed around the $z$axis) from the sensor measurement space onto the filter state space by means of its exact linearization. In this way, the resultant h is the identity function and H_t is an identity matrix. This transformation preserves the higher order statistical effects, improving the Kalman filter performance [10]. Naturally, this means that the R_t matrices corresponding to each information sources must be estimated very accurately in order to have a proper Kalman-filtering-based fusion. The measurement noise covariance matrices corresponding to the IMU and the vehicle measurements are time invariant and are denoted as R^{IMU} and $R^{vehicle}$, respectively. The noise covariance matrix associated with the virtual measurement, provided by the map of elevations, is denoted as R_t^{map} and is time variant.

The IMU provides observations that allow updating the pose, steer angle and vibration's variance components of the observational vector $\vec{z}_t^{IMU}$. The orientation measurements θ_t^{IMU}, ϕ_t^{IMU}, and ψ_t^{IMU} are used directly to update $\vec{q}_t^{IMU}$:

$$\vec{q}_t^{IMU} = q_{YPR}\left(\psi_t^{IMU}, \phi_t^{IMU}, \theta_t^{IMU}\right) \tag{10}$$

with q_{YPR} given by Eq. (8)

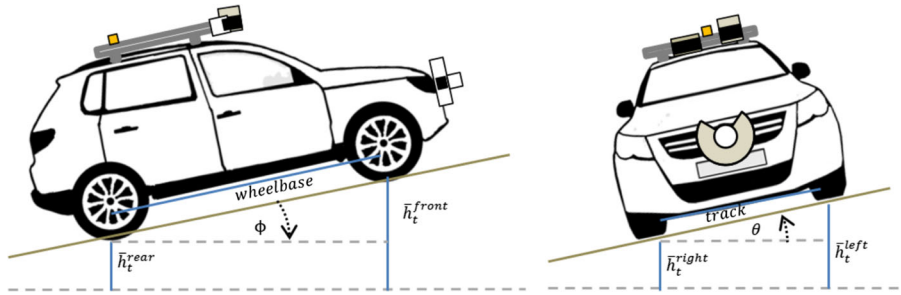

Fig. 3 Rotation angles around the x and y axes

By using Eq. (6), the observation of the steering wheel angle is obtained from the IMU angular speed around the z axis, ω_t^z, as:

$$\alpha_t^{IMU} = \frac{\omega_t^z}{v_t \cdot \gamma} \tag{11}$$

The quantification of the vehicle vibration in the z axis is estimated as the variance of the IMU's acceleration in the z axis:

$$\eta_t^{IMU} = \frac{\sum_{i=0}^{N_f-1} \left(a_{t-i}^z - \bar{a}_t^z\right)^2}{N_f} \tag{12}$$

with N_f the number of samples and $\bar{a}_t^z$ the mean value of the acceleration in the z axis in the same period.

Finally, $\vec{z}_t^{\,IMU}$ is given by[2]:

$$\vec{z}_t^{\,IMU} = \begin{pmatrix} * \\ \vec{q}_t^{\,IMU} \\ * \\ \alpha_t^{IMU} \\ \eta_t^{IMU} \end{pmatrix} \tag{13}$$

The vehicle provides measurements that allow updating the speed and steering wheel angle components of the observational vector $\vec{z}_t^{\,vehicle}$. Given that the vehicle's internal sensors directly provide the speed of the four wheels and the angle of the steering wheel $\vec{z}_t^{\,vehicle}$ has the following form:

$$\vec{z}_t^{\,vehicle} = \begin{pmatrix} * \\ * \\ 1/2(v_t^{vehicle,rl} + v_t^{vehicle,rr}) \\ \alpha_t^{vehicle} \\ * \end{pmatrix} \tag{14}$$

[2]We use "*" to indicate that this component of the observation vector does not exists and, therefore, it is not used in the corrective stage.

with $v_t^{vehicle,rl}/v_t^{vehicle,rr}$ the speed of the rear-left /rear-right wheel.

The map of elevations provides virtual observations that allow updating the vehicle pose components of the observational vector $\vec{z}_t^{\,map}$. Let h_t^{rl}, h_t^{rr}, h_t^{fl} and h_t^{fr} be the heights of the rear-left, rear-right, front-left and front-right wheels, respectively. These heights are obtained by evaluating the terrain map ($map_{height}[\cdot][\cdot]$ array defined in Eq. (22)), with the normalized x and y coordinates of the contact point of the wheels on the ground (see details in Section 3.6). Then, the rotation angles around the x and y axes are given by (see Fig. 3 for details):

$$\begin{aligned} \phi_t^{map} &= a\sin\left(\frac{\bar{h}_t^{rear} - \bar{h}_t^{front}}{wheelbase}\right) \\ \theta_t^{map} &= a\sin\left(\frac{\bar{h}_t^{left} - \bar{h}_t^{right}}{track}\right) \end{aligned} \tag{15}$$

with $\bar{h}_t^{rear} = \left(h_t^{rl} + h_t^{rr}\right)/2$, $\bar{h}_t^{front} = \left(h_t^{fl} + h_t^{fr}\right)/2$, $\bar{h}_t^{left} = \left(h_t^{fl} + h_t^{rl}\right)/2$ and $\bar{h}_t^{right} = \left(h_t^{fr} + h_t^{rr}\right)/2$.

Fig. 4 AMTC's Autonomous Vehicle

Table 1 Vehicle model parameters (Volkswagen®Tiguan)

E	Petrol Engine 4-cylinders 2.0L 125KW (16V) Turbo FSI	
M	Mass	1590[Kg]
I_{zz}	Moment of Inertia with respect to z-axis	2695[Kg·m^2]
l_f	Distance from front axle to CoG position (wrt. x-axis)	1.302[m]
l_r	Distance from rear axle to CoG position (wrt. x-axis)	1.302[m]
C_f	Characteristic curves of the front tires	7791[Kg· m/s(rad)]
C_r	Characteristic curves of the rear tires	7791[Kg· m/s(rad)]
ρ	Atmospheric density	1.225[Kg/m^3]
ε	Aerodynamics coefficient	0.33
A	Frontal area	3.049974[m^2]
	Spin rate steering wheel–tire	1/14.7
	Acceleration 0-100 [km/h]	10.4[s]
μ	Dry pavement friction coefficient	0.8

Finally, $\vec{z}_t^{map}$ is given by:

$$\vec{z}_t^{map} = \begin{pmatrix} * \\ q_{YPR}\left(\psi_t, \phi_t^{map}, \theta_t^{map}\right) \\ * \\ * \\ * \end{pmatrix} \tag{16}$$

with q_{YPR} given by Eq. (8), and ψ_t the current estimation of the rotation angle around z.

The noise covariance matrix associated to the virtual measurement provide by the map of elevations R_t^{map}, is computed as:

$$R_t^{map} = \begin{bmatrix} 0 & 0 & 0\,0\,0 \\ 0 & R_{t,q}^{map} & 0\,0\,0 \\ 0 & 0 & 0\,0\,0 \\ 0 & 0 & 0\,0\,0 \\ 0 & 0 & 0\,0\,0 \end{bmatrix} \tag{17}$$

Table 2 AMTC's Autonomous Vehicle sensors

Sensor Type	Model
LIDAR	SICK, LMS291-S05
LIDAR	SICK, LMS151
LIDAR	SICK, LD-MRS HD
IMU	Crossbow, NAV440
CAMERA	AVT, Manta G046C
CAMERA	Sony, PlayStation®Eye Camera
RADAR	Delphi, ESR
CAN Interface	Kvaser, Leaf Light HS

$$\text{with} \quad R_{t,q}^{map} = \begin{bmatrix} 1\,0\,0\,0 \\ 0\,1\,0\,0 \\ 0\,0\,1\,0 \\ 0\,0\,0\,1 \end{bmatrix} \cdot \max\left(\chi_t^{fl}, \chi_t^{fr}, \chi_t^{rl}, \chi_t^{rr}\right) \tag{18}$$

where χ_t^{fl}, χ_t^{fr}, χ_t^{rl} and χ_t^{rr} are the variances associated to the heights of the rear-left, rear-right, front-left and front-right wheels, respectively. These values are

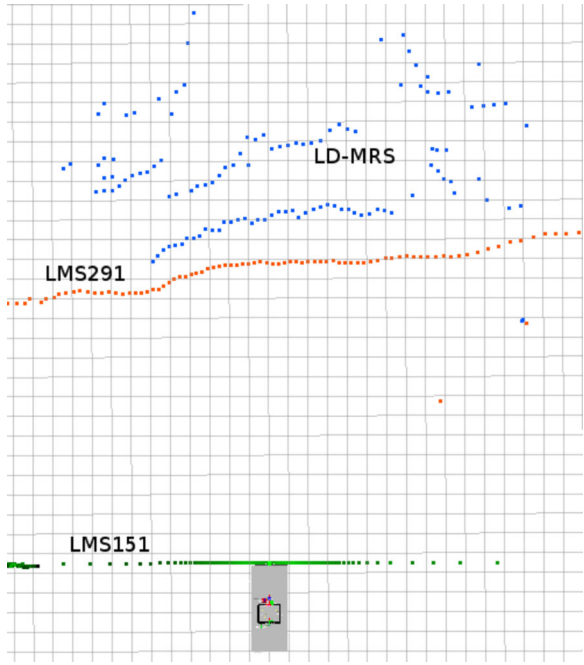

Fig. 5 Example of measurements obtained by the LMS151 (green), LMS291 (red) and LD-MRS (blue) laser rangefinders

Fig. 6 **a** Satellite view of the unpaved road, **b** Example of pictures of the road and **c** laser rangefinder data used as ground truth. Source: Google Maps satellite image

obtained by evaluating the variances of the terrain map ($map_{var}[\cdot][\cdot]$ array defined in Eq. (23)), with the normalized x and y coordinates of the contact point of the wheels on the floor (see details in Section 3.6).

The noise covariance matrices R^{IMU} and $R^{vehicle}$ are estimated in a standard sensor calibration process.

3.5 Laser Projection

The laser measurements are acquired in polar coordinates, relative to the laser rangefinder device (see Subsection 3.3). In order to integrate laser measurements acquired at different times, by one or more different laser rangefinders, measurements are first transformed into Cartesian coordinates, then projected onto the local reference system S_L, and finally onto the global reference system S_G. For the first projection, it is necessary to know the laser pose in S_L, whichis given by the 3D vector $\vec{p}^{\,S_L}_{laser}$ and the quaternion $\vec{q}^{\,S_L}_{laser}$. The vehicle's pose is used for the second projection.

Table 3 Recording's characteristics

Recording ID	Ground Class	Speed Range	Weather Condition
1-2	Unpaved	Low	sunny/dry
3-6	Unpaved	Medium	sunny/dry

Thus, the laser measurements $\vec{\rho}^{\,S_G}_{t,i} \in \mathbb{R}^3$ are obtained as:

$$\vec{\rho}^{\,laser}_{t,i} = \left[\, d_{t,i} \cdot \cos\left(\theta_{t,i}\right) \;\; d_{t,i} \cdot \sin\left(\theta_{t,i}\right) \;\; 0 \,\right]^T; \quad i \in \left\{1, ..., N_{samples}\right\} \tag{19}$$

$$\vec{\rho}^{\,S_G}_{t,i} = \left(x^{S_G}_{t,i} \;\; y^{S_G}_{t,i} \;\; z^{S_G}_{t,i} \right)^T = \vec{q}_t \cdot \left(\vec{q}^{\,S_L}_{laser} \cdot \vec{\rho}^{\,laser}_{t,i} \cdot (\vec{q}^{\,S_L}_{laser})^* + \vec{p}^{\,S_L}_{laser} \right) \cdot (\vec{q}_t)^* + p_t; \; i \in \left\{1, ..., N_{samples}\right\} \tag{20}$$

For each laser measurement, the variance of the measurement, $\chi_{t,i}$, is computed. The two main factors affecting this value are: the measured distance $d_{t,i}$ and the variance of the vehicle's vibration in the z axis. Then, $\chi_{t,i}$ is given by:

$$\chi_{t,i} = \kappa_d \cdot d^2_{t,i} + \kappa_\eta \cdot \eta_t + \kappa_{base} \tag{21}$$

where: κ_d, κ_η, and $\kappa_{base}$are adjusting factors empirically set to 0.04, 0.5 and 0.1, respectively.

3.6 Terrain Map Update

The terrain map is organized as a 2.5D height map, composed by cells of size $M_x \cdot M_y$ [m^2]. The laser measurements $\vec{\rho}^{\,S_G}_{t,i}; i \in \left\{1, ..., N_{samples}\right\}$ are stored in the map. Since more than one laser measurement

can be mapped onto the same cell and that laser measurements corresponding to different time instants can also be mapped onto the same cell, the variance of the laser measurement is considered in the fusion process. Hence, the map stores two values in each cell position: the measured height, map_{height}, and the variance of the measurement, map_{var}. By assuming that laser measurements and map height estimation have Gaussian distributions, they can be optimally fused using a Kalman filtering approach [14]. Thus, in each map cell position$(X_{t,i}, Y_{t,i})$, a 1D Kalman filter estimates the state variable (map height) and its variance as:

$$map_{height}[X_{t,i}][Y_{t,i}] = \frac{\chi_{t,i} \cdot map_{height}[X_{t,i}][Y_{t,i}] + map_{var}[X_{t,i}][Y_{t,i}] \cdot z_{t,i}^{S_G}}{map_{var}[X_{t,i}][Y_{t,i}] + \chi_{t,i}}; i \in \{1, ..., N_{samples}\} \tag{22}$$

$$map_{var}[X_{t,i}][Y_{t,i}] = \frac{map_{var}[X_{t,i}][Y_{t,i}] \cdot \chi_{t,i}}{map_{var}[X_{t,i}][Y_{t,i}] + \chi_{t,i}}; i \in \{1, ..., N_{samples}\} \tag{23}$$

where $X_{t,i} = x_{t,i}^{S_G}/M_x$ and $Y_{t,i} = y_{t,i}^{S_G}/M_y$ are normalized cell coordinates.

4 Experimental Results

4.1 AMTC Autonomous Vehicle

The Advanced Mining Technology Center (AMTC) of University of Chile developed an autonomous vehicle whose final goal is autonomous navigation inside open pit mines. For this application typical truck speeds are in the range of 5-14 [m/s] and navigation based on pure GPS is not reliable, because insome deep sections of the pit GPS signal is not always available. Therefore, robust terrain mapping systems are of high interest.

The AMTC autonomous vehicle corresponds to a standard Volkswagen Tiguan 2010 (see picture in Fig. 4). The roof rack has aluminum-extruded profiles installed for mounting sensors. The vehicle parameters are presented in Table 1. A list of installed sensors is presented in Table 2. The original Tiguan vehicle was mechanically and electronically modified in order to make it autonomous. The modifications can be outlined as follow: the steering wheel is actuated by a brushless motor connected by a chain to the steering column therefore both rotate synchronously. The brake pedal is pulled by a steel rope, which is moved by a linear actuator, placed on the co-pilot's footrest. The control hardware of the accelerator pedal and handbrake were modified, therefore both devices are electronically controlled. The vehicle's internal sensors data is directly acquired from the CAN bus interface. A rack with electronic controllers and computers was installed in the vehicle's trunk. The data acquisition and control routines run on an automotive standard Intel i7 610E @2.53GHz (4GB RAM) computer running ROS-Fuerte on Ubuntu 12.04. More details on the control modules used in this vehicle can be found in [15, 16].

4.2 Evaluation Dataset

Evaluation data was recorded inside O'Higgins Public Park, located near downtown area in Santiago de Chile, Chile. The aforementioned data were captured while the vehicle was driven on unpaved, rough terrain at low (<10 [m/s]) and medium speeds (<20[m/s]). Each recording have measurements from three laser rangefinders, one IMU, one radar, two cameras, one GPS and the vehicle's CAN bus data (see device's models in Table 2).

As explained previously, the terrain map is built using the laser measurements. The SICK LMS291 and LMS151 rangefinders have one scanning plane while the SICK LD-MRS HD has four scanning planes. The three laser rangefinders are placed with different and fixed pitch angles, thus are capable of taking measurements at different distances in front of the vehicle. The SICK LMS291's scanning plane touches the floor at 16 [m] in front of the vehicle, while the SICK

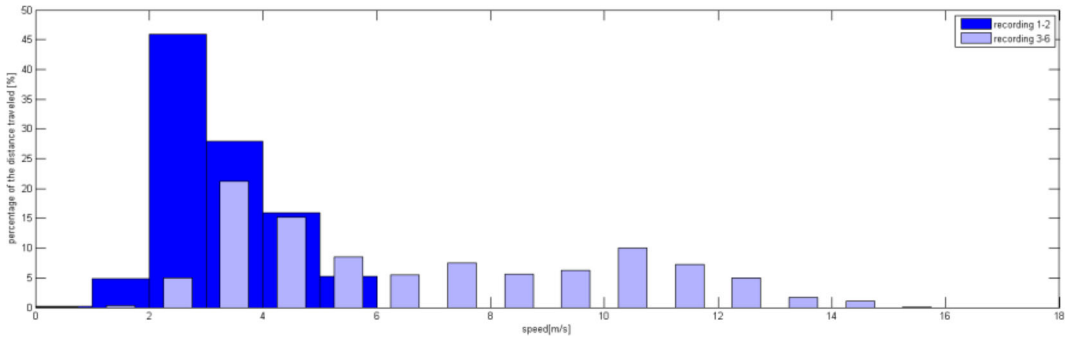

Fig. 7 Percentage of the total traveled distance versus the vehicle's speed for recordings 1-2 and 3-6

LD-MRS's inferior scanning plane touches the floor at 19[m] in front of the vehicle. The SICK LMS151 is mounted vertically pointing to the floor. This sensor is used as ground truth for the map's integration. An example of the laser measurements is shown on Fig. 5.

The unpaved area is formed by a very irregular road having a length of about 800 [m] with positive and negative slopes (see Fig. 6a). The road is a track made of ground surrounded with grass and some trees. The height difference between the lowest and the highest point of the track is about 4 meters. In this area six recordings with different speed ranges and driving directions were taken as shown in Table 3. Figure 7 shows the speed distribution of those recordings. The average speed for recordings 1-2 is 2.91 [m/s] while the average speed for recordings 3-6 is 5.40 [m/s].

4.3 Experiments

The proposed Kalman-based terrain estimation methodology is compared against a baseline methodology, which does not use any state estimator but the IMU and speed information. In addition, the use of the terrain map as virtual observations in the state estimator is analyzed. Thus, the following systems are compared:

- S1 "baseline". The IMU measurements and the vehicle's speed information sources are used in order to obtain the displacement of the vehicle and the pose's change of the laser rangefinders. No Kalman filter is used for estimating the pose of the laser rangefinders or for data fusion in the terrain map.
- S2 "full state estimator". The S2 system is built using the here-proposed methodology, using all information sources.
- S3 "full without map feedback". Same as S2, but without using the feedback of the map as virtual observations in the Kalman filter.

As already mentioned, the measurements obtained by a laser rangefinder mounted vertically on the front of the vehicle are used to build the ground truth. The measurements of this sensor are compared with the corresponding values of map_{height}. Naturally these values are compared using the terrain coordinates.

In order to quantify the map estimation errors, the root square error is measured in each map cell. Then, two quality measures are computed: (i) the Root Mean

Table 4 Experiment results for recordings 1-2 (low speed), normalized by the number of samples (11,602)

	S1	S2	S3
RMSE_{sample}	41.5877 10^{-3}[m]	14.7799 10^{-3}[m]	14.8113 10^{-3}[m]
% Cases better than baseline system	–	81.21%	80.26%

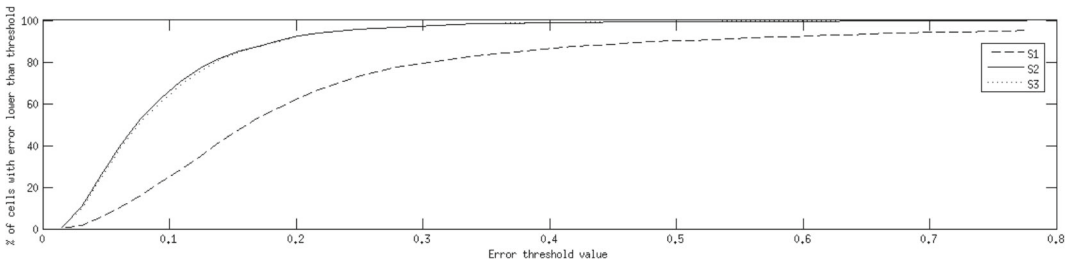

Fig. 8 ROC curves for recording 1-2. % of cells whose root mean square error is lower than a given threshold

Square Error (RMSE) over the whole map, normalized by the number of samples ($RMSE_{sample}$) and (ii) the percentage of map cells which root square error is lower than a given threshold value. Using several different threshold values, Receiver Operating Curves (ROCs) are built. In addition, the percentage of cases in which the proposed system (S2) or a variant (S3) has a lower $RMSE_{sample}$, than the baseline system (S1) is calculated.

In the first experiment, the systems were compared using recording 1 and 2 (low speed). Table 4 shows the obtained $RMSE_{sample}$ and Fig. 8 shows the ROC curves of the error. It can be observed that the systems that use the state estimators (S2 and S3) obtained a much lower error in the map compared to the baseline system (S1); the $RMSE_{sample}$ of systems S2 and S3 is 35 % of the one of S1. Table 4 also shows that in approximately 80 % of the map cells (81.21 % for S2 and 80.26 % for S3), the height estimations of the systems that use the state estimators (S2 and S3) have a lower error than the ones of the baseline system. Furthermore, in Table 4 it can be observed that best results are obtained when all information sources are used in the state estimator (S2); a slightly higher $RMSE_{sample}$ is obtained when the terrain map data is not used in the state estimation.

In the second experiment, the systems were compared using recordings 3-6 (medium speed). Table 5 shows the obtained $RMSE_{sample}$ and Fig. 9 displays the ROC curves of the error. As in the first experiment, it can be observed that the systems that use the state estimators (S2 and S3) obtained a much lower RMSE in the map compared to the baseline system (S1). In fact, the RMSE is reduced by approximately one third Table 5 shows that in about 60 % of the map cells (63.18 % for S2 and 59.95 % for S3), the height estimations of the systems that use the state estimators (S2 and S3) have a lower error that the ones of the baseline system. As in experiment 1, in Table 5 it can be observed that the best results are obtained when all information sources are used in the state estimator (S2); a 10 % higher $RMSE_{sample}$ is obtained when the terrain map data is not used in the state estimation.

It is worth to mention that in addition to the reported experiments in unpaved, rough terrain, several experiments were carried out in paved roads at different speeds, in order to estimate the minimal error that the terrain map estimation system can have. The minimal RMSE is 10.1 10^{-3}[m], which is of the same order of the RMSE obtained in recordings 1-2. This value is also very close to the theoretical minimum RMSE that can be obtained by such a system, which is given by the angular projections of the laser range finder variance:

$$\mathrm{E}\,[RMSE] = \sqrt{\sum_{i=1}^{N} \cos(\alpha_i)^2 \cdot \sigma^2_{sensor} \Big/ N} \qquad (24)$$

with α_i the sweep angle of the sensor and N the number of measurements.

Table 5 Experiment results for recordings 3-6 (medium speed) normalized by the number of samples (11,904)

	S1	S2	S3
$RMSE_{sample}$	78.990 10^{-3}[m]	52.4298 10^{-3}[m]	57.8229 10^{-3}[m]
% Cases better than baseline system	–	63.18%	59.95%

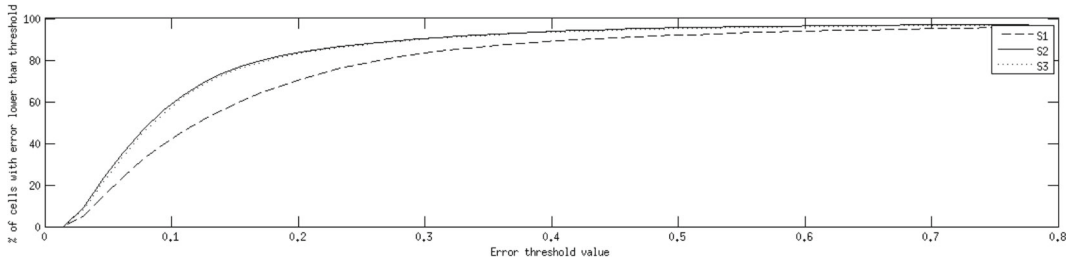

Fig. 9 ROC curves for recording 3-6. % of cells whose root square error is lower than a given threshold

Finally, it is important to stress that the two estimation systems derived from the application of the proposed methodology (S2 and S3) work on-line and in real-time. Table 6 shows the processing time of each stage, when it is executed. These processing times were measured using the main computer of the AMTC autonomous vehicle (See Section 4.1).

The prediction step of the Vehicle Estimation Stage is executed at a framerate of 200 [Hz]. The correction step is executed asynchronously everytime the IMU the internal sensors of the vehicle or the map updating process generate new data. The IMU and the internal sensors generate data at the following rates: IMU at 100 [Hz], angle of the steering wheel at 50 [Hz], and linear speed of the wheels at 50 [Hz]. The map updating process generates data at a framerate of 10 [Hz].

The Laser Projection Stage and the Terrain Map Update are also executed asynchronously everytime the laser range finders generate new data. These sensors generate data at the following rates: LMS 291 laser range finder at 75 [Hz] and LD-MRS laser range finder at 50 [Hz].

Table 6 Processing time of the estimation process

	Processing Time [10^{-6} s]	Number of times that the module is called in a second
Vehicle State Estimation (Prediction Step)	0.5	200
Vehicle State Estimation (Correction Step)	122.6	210
Laser Projection	87.1	125
Terrain Map Update	104.0	125

5 Conclusions

The accurate and real-time generation of terrain maps in off-road, irregular terrains is addressed in this work. The proposed methodology is based on the use of an Extended Kalman filter for estimating in real-time the instantaneous pose of the vehicle and the laser rangefinders by considering measurements taken from an inertial measurement unit, internal sensorial data of the vehicle and the estimated heights of the four wheels, which are obtained from the terrain map and allow determining the vehicle's inclination. The estimated 6D pose of the laser rangefinders is used to correctly project the laser measurements onto the terrain map. The terrain map is a 2.5D map that stores the mean value and variance of the terrain height. In each map's cell position, new laser observations are fused with existing height estimations using a Kalman filter.

The methodology is validated in the real world (O'Higgins Public Park, located near downtown area in Santiago de Chile, Chile), using an autonomous vehicle. The evaluation dataset was captured while the vehicle was moving on unpaved, rough terrain at low and medium speeds, for 4.8 [km].

Experiments show that the use of the proposed methodology allow to increase the quality of the obtained maps; the RMSE is reduced to one third in the case that the vehicle is moving at low speeds, and reduced to two thirds when the vehicle is moving at medium speeds. Furthermore, it can be observed that in most of the map's cells (80 %/60 % in case the vehicle is moving at low/medium speeds), the height estimations are more accurate when the Kalman-filter-based methodology is used.

In addition, experiments show that the use of the map heights for the estimation of the pose of the laser rangefinders allow obtaining more accurate

maps. When the map heights are not used, the RMSE increases by approximately 10 %, when the vehicle is moving at medium speeds.

Acknowledgments This research was partially supported by FONDECYT (Chile) under Project Number 1130153.

Appendix 1

From Fig. 2a, it can be observed that:

$$\sin(\alpha_t) = \frac{wheelbase}{r_t} \tag{25}$$

Then, given that $v_t = \omega_t \cdot r_t$, the following expression for w_t is obtained:

$$w_t = \frac{v_t \sin(\alpha_t)}{wheelbase} \tag{26}$$

The following linear approximation between the steer angle α_t and the angle of the steering wheel α_t^{wheel} is used:

$$\alpha_t \simeq \beta \cdot \alpha_t^{wheel} \tag{27}$$

with β a real number. Figure 10 shows the linear relationship obtained for the Volkswagen Tiguan used in this work.

Finally, from Eqs. (26) and (27), and considering that α_t is small, the final expression for w_t is defined as:

$$w_t \simeq \frac{v_t \cdot \beta \cdot \alpha_t^{wheel}}{wheelbase} \simeq v_t \cdot \alpha_t^{wheel} \cdot \gamma \tag{28}$$

with γ a real number. For the Volkswagen Tiguan, $\gamma = 0.02359 \left[\frac{1}{m}\right]$ is obtained by a linear regression.

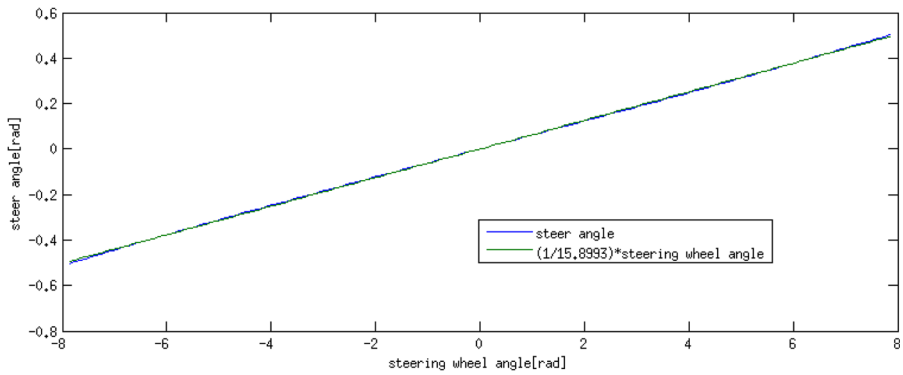

Fig. 10 Relationship between the steer angle and the angle of the steering wheel, for the Volkswagen Tiguan vehicle

References

1. Jazar, R.N.: Vehicle Dynamics: Theory and Application, p. 1015. Springer (2008)
2. Stavens, D., Thrun, S.: A self-supervised terrain roughness estimator for off-road autonomous driving. In: Proceedings of Conference on Uncertainty in AI, pp. 13–16 (2006)
3. Hadsell, R., Bagnell, J.A., Huber, D., Hebert, M.: Accurate rough terrain estimation with space-carving kernels. In: Proceedings of the 2009 Robotics: Science and Systems Conference - RSS 2009, Washington (2009)
4. Hebert, M., Caillas C., Krotkov, E., Kweon, I.S., Kanade, T.: Terrain mapping for a roving planetary explorer. In: Proceedings of International Conference on Robotics and Automation (ICRA), vol. 2, pp. 997–1002 (1989)
5. Pfaff, P., Triebel, R., Burgard, W.: An efficient extension to elevation maps for outdoor terrain mapping and loop closing. Int. J. Robot. Res. **26**(2), 217–230 (2007)
6. Chen, T., Dai, B., Wang, R., Liu, D.: Gaussian-process-based ground segmentation for autonomous land vehicles. J. Intell. Robot. Syst. (In press)
7. Shin, Y., Jung, Ch., Chung, W.: Drivable road region detection using a single laser range finder for outdoor patrol robots. In: Proceedings of the 2010 IEEE Intelligent Vehicles Symposium, University of California, San Diego, pp. 21–24 (2010)
8. Ye, C., Borenstein, J.: A new terrain mapping method for mobile robots obstacle negotiation. In: Proceedings of the UGV Technology Conference at the 2002 SPIE AeroSense Symposium. pp. 21–25 (2003)
9. Gu, J., Cao, Q., Huang, Y.: Rapid traversability assessment in 2.5D grid-based map on rough terrain. Int. J. Adv. Rob. Syst. **5**(4), 389–394 (2008)
10. Miller, I., Campbell, M.: A mixture-model based algorithm for real-time terrain estimation. J. Field Robot. **23**(9), 755–775 (2006)
11. Qiu, Q., Yang, T., Han, J.: A new real-time algorithm for off-road terrain estimation using laser data. Sci. China Ser. F: Inf Sci. **52**(9), 1658–1667 (2009)
12. Tse, R., Ahmed, N., Campbell, M.: Unified mixture-model based terrain estimation with Markov Random Fields. In: Proceedings of the 2012 IEEE International Conference On Multisensor Fusion and Integration for Intelligent Systems. Germany (2012)
13. Thrun, S., Montemerlo, M., Dahlkamp, H., Stavens, D., Aron, A., Diebel, J., Fong, P., Gale, J., Halpenny, M., Hoffmann, G., Lau, K., Oakley, C., Palatucci, M., Pratt, V., Stang, P., Strohband, S., Dupont, C., Jendrossek, L.-E., Koelen, C., Markey, C., Rummel, C., van Niekerk, J., Jensen, E., Alessandrini, P., Davies, B., Ettinger, S., Kaehler, A., Nefian, A., Mahoney, P.: Stanley: The robot that won the DARPA grand challenge. J. Field Robot. **23**, 661–692 (2006)
14. Welch, G., Bishop, G.: An Introduction to the Kalman Filter. University of North Carolina at Chapel Hill, NC (1995)
15. Bernuy, F., Ruiz-del-Solar, J., Parra-Tsunekawa, I., Vallejos, P.A.: Adaptive and real-time unpaved road segmentation using color histograms and RANSAC. In: 9th IEEE International Conference on Control & Automation - ICCA 2011, pp. 136–141. Santiago (2011)
16. Cabello, F., Acuna, A., Vallejos, P.A., Orchard, M.E., Ruiz-del-Solar, J.: Design and validation of a fuzzy longitudinal controller based on a vehicle dynamic simulator. In: 9th IEEE International Conference on Control Automation - ICCA 2011, pp. 997–1002. Santiago (2011)